DE GRUYTER OPEN

Acta Geophysica
vol. 64, no. 4, Aug. 2016, pp. 1139-1163
DOI: 10.1515/acgeo-2016-0041

Effect of Shale Distribution on Hydrocarbon Sands Integrated with Anisotropic Rock Physics for AVA Modelling: A Case Study

Aamir ALI[1], ZUBAIR[1,2], Matloob HUSSAIN[1], Khaista REHMAN[3], and Muhammad TOQEER[1]

[1]Department of Earth Sciences, Quaid-i-Azam University, Islamabad, Pakistan
e-mail: aamirali.geo@gmail.com

[2]Schlumberger Information Solutions, Ocean Tower, Do Talwar, Karachi, Pakistan

[3]National Centre of Excellence in Geology, University of Peshawer, Pakistan

A b s t r a c t

Shales can be distributed in sand through four different ways; laminated, structural, dispersed and any combination of these aforementioned styles. A careful analysis of well log data is required for the determination of shale distribution in sand affecting its reservoir quality. The objective of this study is to characterize the effect of shale distribution on reservoir quality of sands using well log data. The correlation of well data in terms of lithology has revealed four sand and three shale layers in Lower Goru Formation acting as a major reservoir in the study area. Our results indicate that the laminated type of shale distribution prevails at the Basal sand level, which does not affect its reservoir quality greatly. The remaining layers of variable vertical extent show a variety of shale distribution models affecting their reservoir quality adversely. We also present anisotropic rock physics modelling for AVA analysis at Basal sand level.

Key words: shaly-sands, reservoir properties, shale distribution, rock physics, anisotropic AVA modelling.

1. INTRODUCTION

Shales are the most common type of sedimentary rocks present in the Earth's crust. In the context of hydrocarbon exploration, shales are considered as source as well as cap rocks (Sunjay 2011).The presence of shale in porous formations causes problems for interpretation of wireline logs. This is not only due to the gross effect of shale on porosity values, but it can also affect the final calculated original gas in place (OGIP) for a given formation. In most cases, the reservoir sands contain some degree of shaliness which may adversely affect the reservoir quality (Paul 2012). However, physical properties, volume, and distribution of shale are major affecting candidates that may mislead the log reading and consequent interpretation (Clavier *et al*. 1984, Waxman and Smith 1968).

Shales are distributed in sand through four different ways, called laminated, structural, dispersed, and any combination of them (Clavaud *et al*. 2005, Sams and Andrea 2001). The best and common indicator of shale using the well log data is gamma ray (GR) log (Asquith *et al*. 2004, Tiab and Donaldson 2003, Zinszner and Pellerin 2007). This log responds to the changes in natural gamma radiation emitted by the formation. In shaly-sands the level of gamma radiation emitted is generally a function of clay volume only. The gamma ray log does not measure the volume of silts or other inclusions within the shales (Asquith *et al*. 2004, Tiab and Donaldson 2003). Although the gamma ray log is often the best shale indicator available, it is not definitive in identifying the sand-shale boundary by itself. In radioactive sands, gamma ray indicates shale, but responds as sand on neutron and density logs (Minh *et al*. 2008).

The objective of this study is to characterize the effect of shale distribution on reservoir quality of sands encountered in Lower Goru Formation using well log data of Khipro area, Lower Indus Basin, Pakistan. A further aim is to present anisotropic rock physics based amplitude *versus* angle (AVA) model to investigate amplitude variations for reservoir sand in the study area. The data used for this study consists of common suite of wireline logs, recorded in wells of Bilal-01, Inam-Basal-01, Siraj-South-01, and Naimat-Basal-01 with their location and detail given in Fig. 1 and Table 1, respectively. Different logs such as gamma ray, spontaneous potential, resistivity, sonic, porosity, and density were analyzed and interpreted in order to define reservoir geometry and properties. For the accomplishment of the above objectives, the workflow followed in the study for the determination of effect of shale distribution on hydrocarbon sands in Khipro block (study area) is given in Fig. 2. The workflow for the anisotropic rock physics AVA modelling will be presented and discussed in the Section 5.

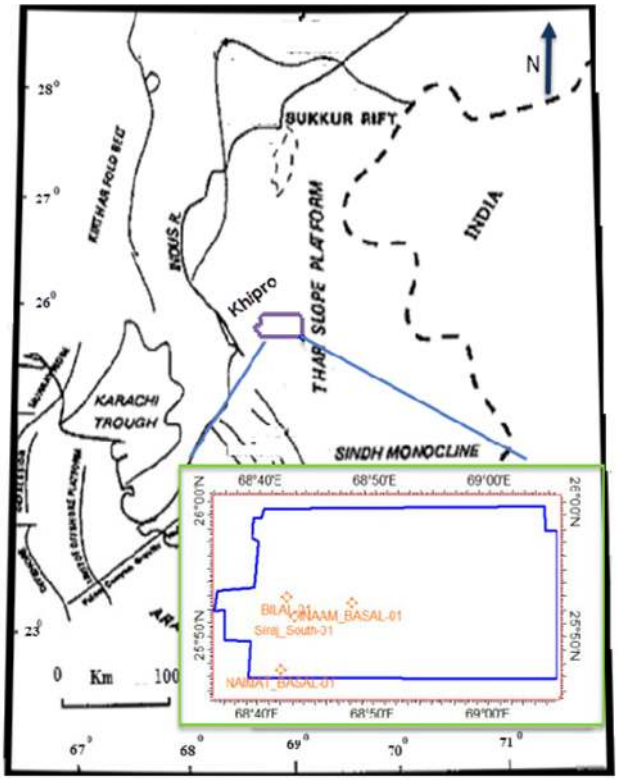

Fig. 1. Map showing the location of Khipro block and wells used in this study (Bender and Raza 1995).

Table 1

Well data used for research work

Well name	Formation top [m]				Well total depth [m]	Status of well	Discovery
	Upper sand	Middle sand	Sand above Talhar Shale	Basal sand			
Siraj South-01	3383	2597	2905	3055	3218	Exploratory	Gas condensate
Bilal-01	2385	2605	2929	3058	3170	Exploratory	Gas condensate
Naimat Basal-01	2311	3000	3389	3479	3599	Exploratory	Gas condensate
Inam Basal-01	2261	2445	2665	2955	3153	Exploratory	Gas condensate

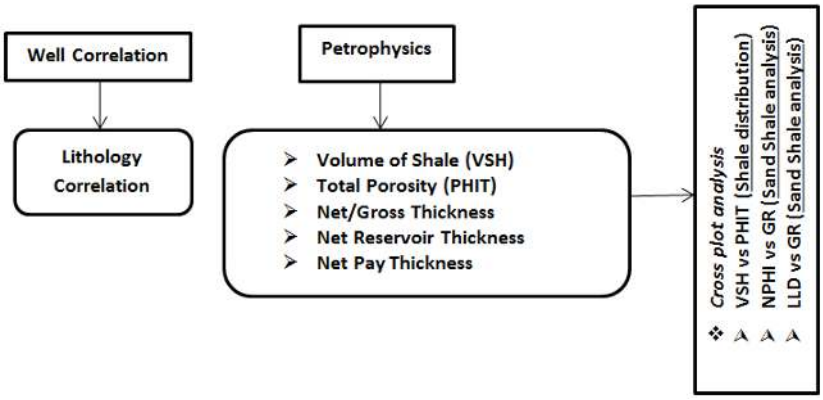

Fig. 2. Workflow followed for the determination of effect of shale distribution on hydrocarbon sands in the study area.

2. STUDY AREA

Khipro block is situated between latitude 25°40′N to 26°00′N and longitude 68°20′E to 69°14′E covering an area of 2376 km (Fig. 1). The basinal history of Khipro block is related to rifting and breaks up of Gondwanaland in Jurassic period (Oldham 1982). Khipro lies in Thar platform which is a westward sloping monocline and is controlled by its basement topography (Wandrey *et al*. 2004). After Paleocene there was a continuing oblique convergence of Indian plate and Eurasian plate throughout the Tertiary time and the collision causes tilting of the entire region (Powell 1979).

The presence of Jurassic rocks in area shows deposition during rifting. The rifting has resulted in the formation of normal faulting and horst and grabben structures (Fig. 3). The most important and well developed sedi-

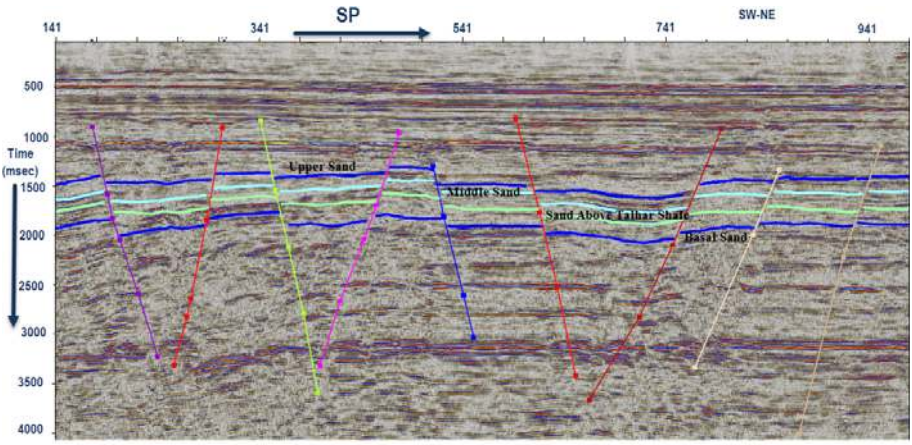

Fig. 3. Existence of normal faults showing start and end of rifting in the study area.

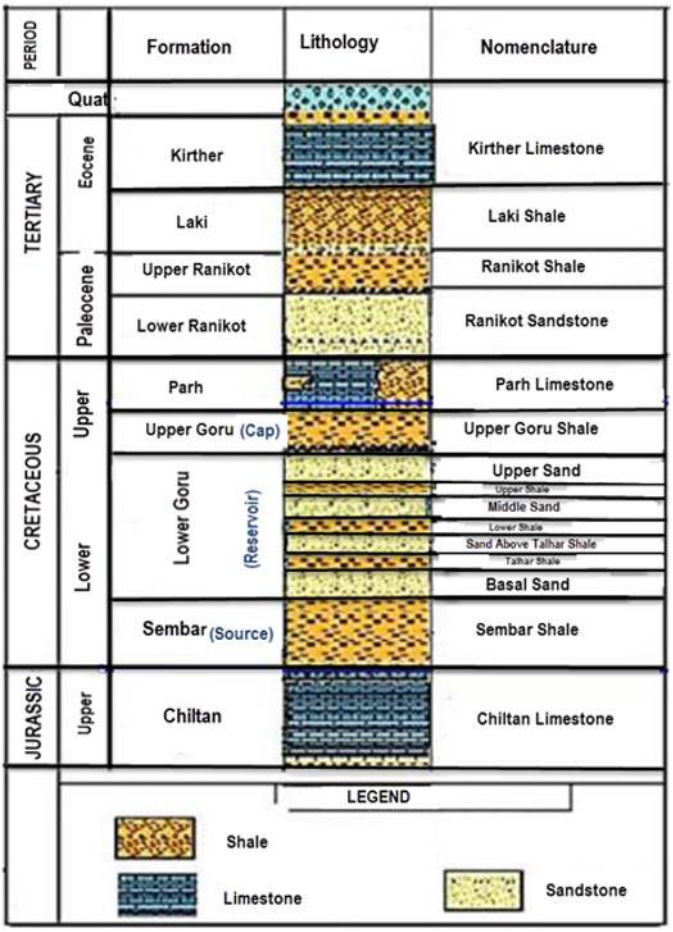

Fig. 4. Stratigraphic chart of the study area showing the petroleum play (Zaigham and Mallick 2000).

mentary rock in this area is Early/Middle Cretaceous sands (Lower Goru Formation) which acts as a good reservoir for oil and gas fields (Ahmad *et al*. 2004). These sands are underlain by shale and marl (Upper Goru) which act as seal for reservoirs (Kazmi and Abbasi 2008). The stratigraphic chart for the study area is given in Fig. 4.

Henceforth we present a brief explanation of workflow followed for characterizing the type of shale distribution in this study.

3. METHODOLOGY

For the determination of effect of shale distribution on hydrocarbon sands in the study area we have used the following methodology divided in three parts:

3.1 Well correlation

Well correlation entails determination of continuity and equivalence of lithological units, particularly reservoir sands or marker sealing shale across a region of the subsurface (Tearpock and Bischke 1991). It is essential to develop a good understanding of the geometry, continuity, and depositional settings of the sediment packages in order to build predictive geological and basin models, and minimize the risk of well target and performance failure (Li *et al*. 2004). Marker bed correlation is the most widely used and treated as reliable correlation technique even if the lithology or origins of the beds are not known (Li *et al*. 2004).

3.2 Petrophysical interpretation for reservoir parameters

Petrophysical interpretation of well logs basically provides us a way to calculate important physical properties like velocity, porosity, volume of shale, water saturation, and hydrocarbon saturation using empirical relations (Akhter *et al*. 2015, Ali *et al*. 2015, Asquith *et al*. 2004, Tiab and Donaldson 2003, Zinszner and Pellerin 2007). In this study, we have followed the workflow presented by Akhter *et al*. (2015) and Ali *et al*. (2015) for the calculation of classical petrophysical properties like velocity, porosity, water saturation, hydrocarbon saturation, and volume of shale.

Furthermore, the analysis of petrophysical logs in this study was also aimed at determining other relevant important reservoir properties (Gross/Net thickness, Net reservoir thickness, Net pay thickness, and Gross porosity) of Lower Goru Sands in Khipro area using cutoff presented in Table 2. Gross/Net thickness is the thickness of a certain facies in that particular zone, net reservoir thickness represents part of net thickness which has a certain amount of porosity, net pay thickness is the thickness contributing to economically viable production, and gross porosity is total porosity.

Table 2

Details of cut-off used for reservoir properties calculation

Cut-off	GR <= 75 API	0.1 <= NPHI <= 0.45	Sw <= 50%
Net thickness [m]	Yes	No	No
Net reservoir thickness [m]	Yes	Yes	No
Net pay thickness [m]	Yes	Yes	Yes

3.3 Distribution of shale in sand

Shales are distributed in sand through four different ways, called laminated, structural, dispersed, and any combination of the above models (Waxman and Smith 1968). Thomas and Stieber (1975) suggested a shale distribution

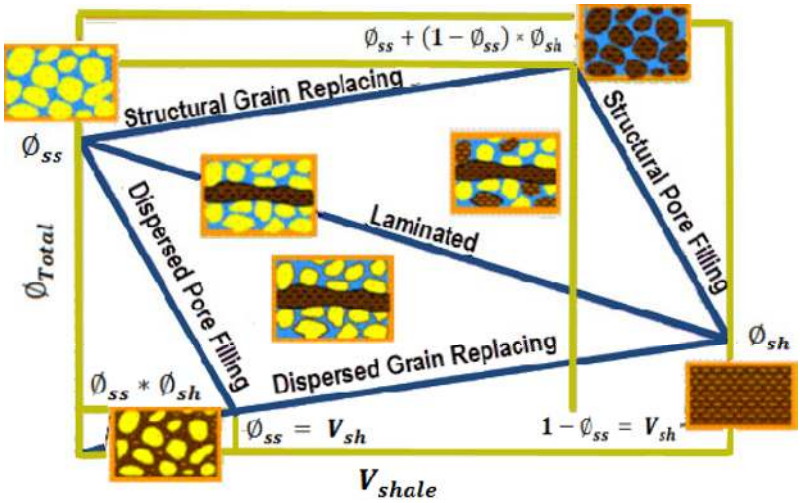

Fig. 5. Shale distribution model proposed by Thomas and Stieber (Tyagi *et al*. 2009). Here V_{shale} is the volume of shale, φ_{total} is the total porosity, φ_{max} is the maximum porosity, and φ_{sh} is the porosity in shale.

model which comprised shale configurations, sand portion, and sand porosity based on volume of shale and porosity (Fig. 5).

Laminar shale is dispersed in reservoir as thin layers of allogeneic clay which does not affect effective porosity, water saturation or horizontal permeability of reservoir rock, but affects the vertical permeability between reservoir rocks (Kurniawan 2005). Laminated shaley-sand repeats sequences of deposition under dual flow regimes considered by dissimilarities in energy levels (Visser 1998).

Dispersed shale is composed of clay minerals that form after deposition because of chemical reactions between minerals and chemicals in formation water due to variety of crystal sizes and shapes (Saxena *et al*. 2006). It significantly decreases the porosity, because shale occupies pore spaces, pore throats, and the water wetness of shale is generally higher than that of sand. Dispersed shale also causes increase in water saturation, reducing resistivity, porosity, and permeability of sands (Kurniawan 2005). The quantity of dispersed shale increasing more than 40% of sand pore space in a reservoir severely affects the pay zones of sands (Visser 1998).

Structural shale is deposited as particles or clasts during early depositional stage (Kurniawan 2005). Although it generally behaves like laminar shale, their permeability, and resistivity properties are similar to the dispersed shale (Kurniawan 2005). It contains shale nodules, which are mixed with sand grains to form part of sandstone having grain size almost same as sand

grains. Structural shales act as framework grains. This may or may not affect reservoir properties by blocking spaces between the grains (Visser 1998).

In most cases, all types of shales are distributed within the sand affecting its reservoir quality in a manner different from each other. Shale distribution can be determined from Thomas–Stieber cross-plot (Fig. 5; Thomas and Stieber 1975, Tyagi *et al*. 2009), where volume of shale (VSH) is plotted on the X-axis and total porosity (PHIT) on the Y-axis. Based on position of data points in the cross plot, laminar, dispersed, structural shale volumes in sand can be recognized and distinguished (Fig. 5).

A common practice is to use the maximum gamma-ray response as the shale point (Heslop 2005). But the mineralogical and compositional heterogeneity of shale may result in a relatively low gamma ray response. For example, sands with kaolinite clays will have a lower gamma ray response as compared to other shaley-sands. It is therefore more accurate to identify the gamma-ray response at the sand-shale boundary (La Vigne *et al*. 1994). Several log combinations may be used to determine the sand-shale boundary, but the most appropriate ones are the laterolog deep resistivity (LLD), neutron porosity (NPHI), and gamma ray (GR) (Heslop 2005). With the help of cross plots between these logs, one can perform detailed sand-shale analysis and also can differentiate between water or gas sand.

4. RESULTS AND DISCUSSION FOR SHALE DISTRIBUTION IN SAND

Lithological correlation of Lower Goru Formation has been prepared by matching formation tops from one well to another (Fig. 6). The lithological units are represented in vertical succession by distinct surfaces which represent changes in lithological character. This correlation has revealed sand layers named as: Upper sand, Middle sand, sand above Talhar Shale, and Basal sand of variable thickness from shale layers named as: Upper shale, Lower shale, and Talhar shale of variable thickness (Fig. 6).

After discriminating between sand and shale bodies, the classical reservoir properties (*e.g*., total porosity, volume of shale, and water saturation) are determined by using petrophysical interpretation for wells Naimat Basal-01 (Fig. 7) and Siraj South-01 (Fig. 8). Other relevant important reservoir properties (gross thickness, net thickness, net reservoir thickness, and net pay thickness) are also determined based on the values of cut-offs presented in Table 2. These reservoir properties for both wells are tabulated in Tables 3 and 4. Based on the results of petrophysical analysis, Upper and Basal sand layers show very good quality reservoir rock, while Middle sand and sand above Talhar shale show poor reservoir quality. Overall, the reservoir qualities of Lower Goru Sands vary from very good to poor. Generally the good or bad quality of reservoir depends mainly on its porosity and permeability.

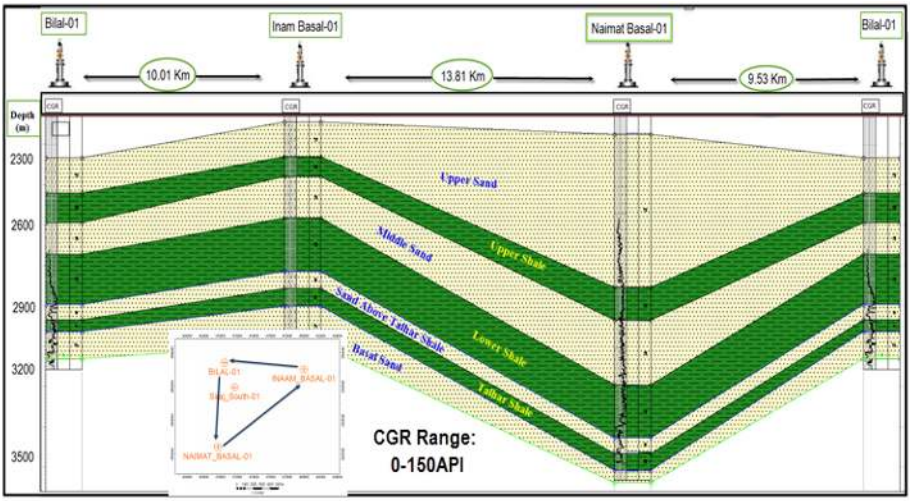

Fig. 6. Well correlation at Lower Goru level.

Here we have tried to describe the reservoir quality in terms of net reservoir thickness and net pay thickness using the cut off values given in Table 2 on classical petrophysical properties. In what follows, the reservoir quality of the sand layers will be related to the type of shale distributed within them.

The type of shale distribution in identified sand packages has been determined from cross-plot of volume of shale (VSH) and total porosity (PHIT) obtained from Siraj South-01 and Naimat Basal-01. Interpretation of this cross-plot on the basis of position of data points indicates that almost all types of shales are distributed within the sand bodies (Figs. 9-12).

Sand above Talhar shale has a small vertical extent (thickness) as compared to all other sand layers with mostly structural along with dispersive shale distribution (Fig. 11). This type of shale distribution in Sand above Talhar shale further affects its reservoir quality along with its small vertical extent. The effect can be in the form of decreased porosity (as dispersive shale occupies pore spaces) and increased water saturation (as water wetness of shale is generally higher than that of sand). The values of porosity and water saturation are used in the cut-off values of net reservoir thickness and net pay thickness.

Middle sand has a large vertical extent as compared to Sand above Talhar shale, but with large distribution of structural and dispersive shales along with some quantity of laminar shale (Fig. 10). Due to the presence of more structural and dispersive shale this sand layer also has a poor reservoir quality as in the case of Sand above Talhar shale.

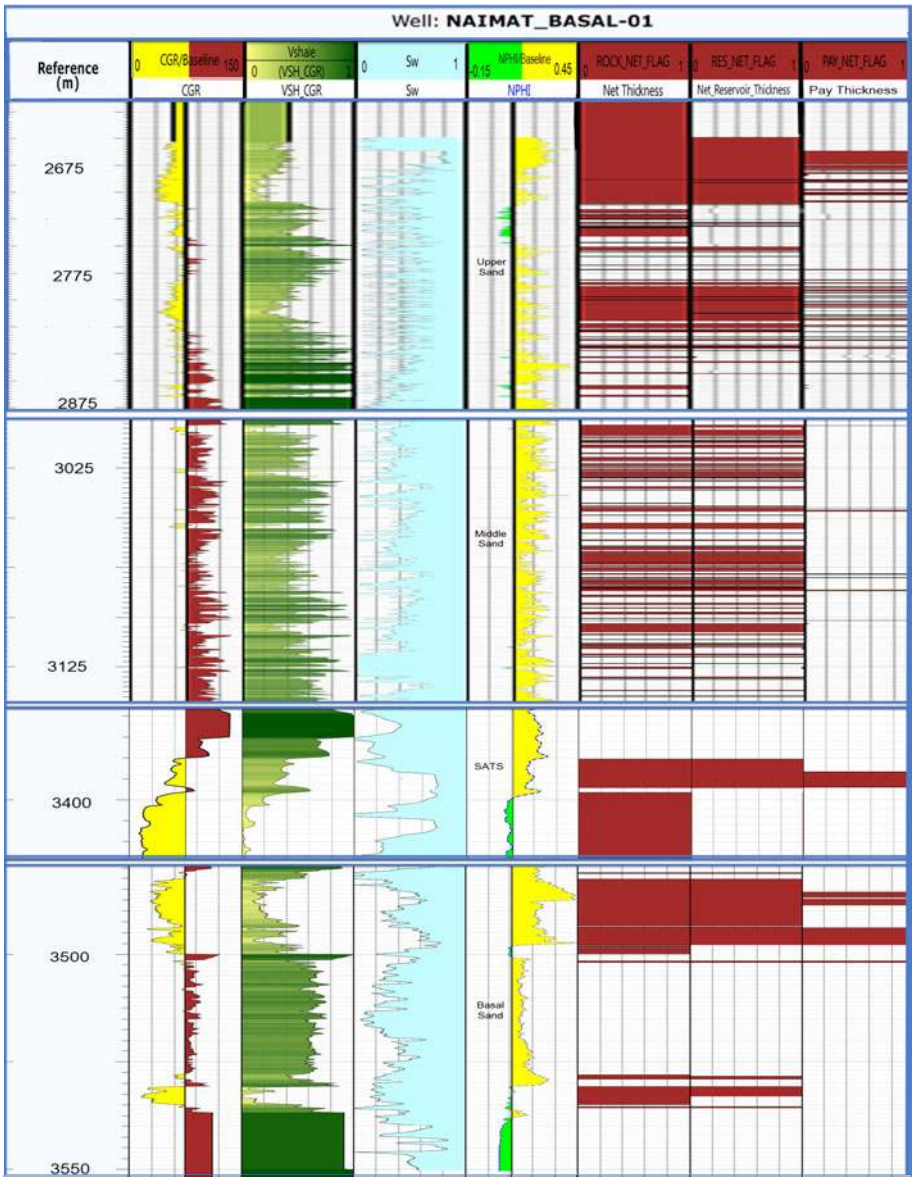

Fig. 7. Petrophysical properties at Lower Goru level for well Naimat Basal-01 with each sand interval shown in different depth scale for better legibility.

Upper and Basal sand layers can be considered as major hydrocarbon bearing sand packages due to their reasonable vertical extent as compared to the other sand layers (Figs. 7-8, Tables 3-4). In geological terms, the sand

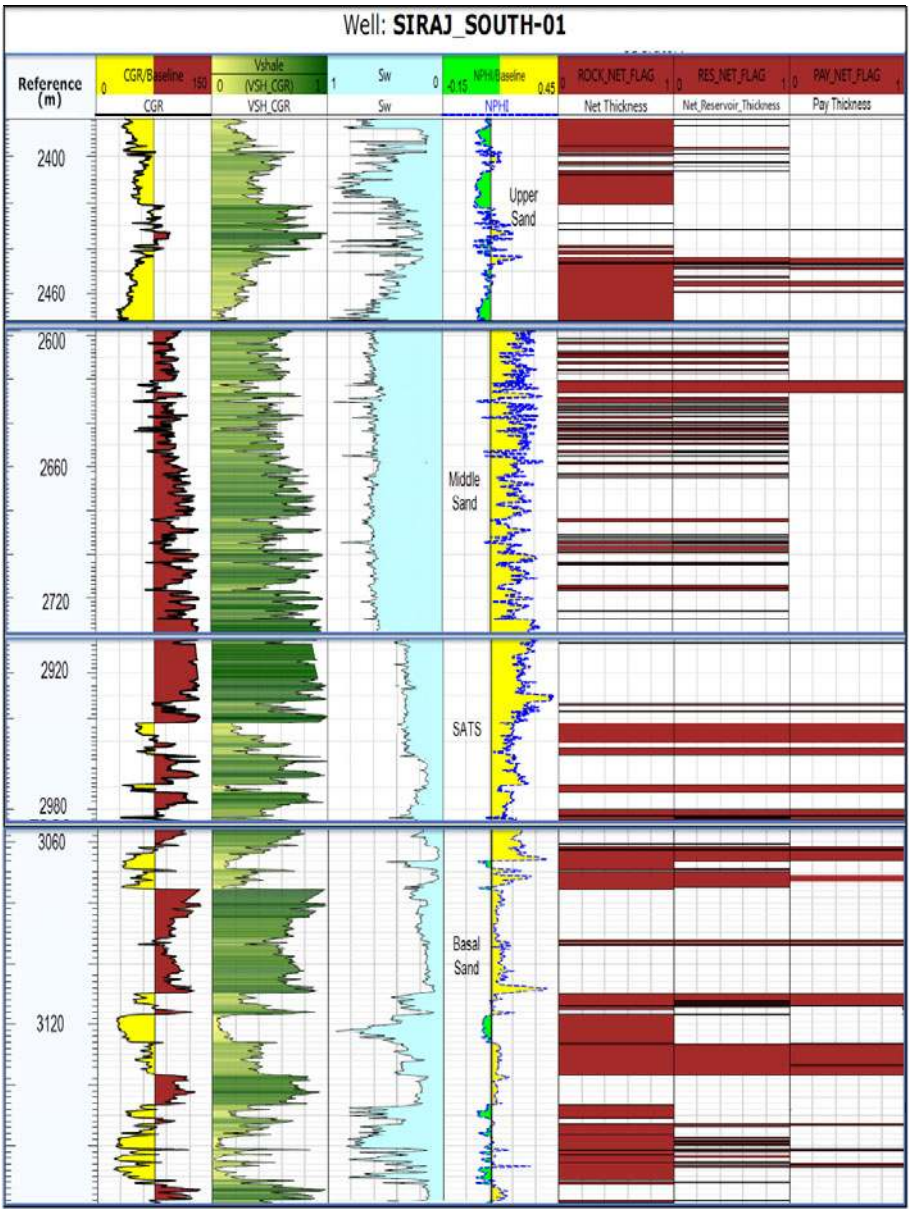

Fig. 8. Petrophysical properties at Lower Goru level for well Siraj South-01.

packages formed in longer deposition time will have a reasonable vertical extent. All types of shales (laminated, structural, and dispersed) are distributed within these layers (Figs. 9 and 12). There is a presence of more dis-

Table 3

Reservoir properties in Lower Goru Sands in Naimat Basal-01 well

Naimat Basal-01	Upper sand	Middle sand	Sand above Talhar Shale	Basal sand
Depth range [m]	2311-2878	3000-3143	3389-3407	3479-3570
Gross thickness [m]	567	144	18	91
Net thickness [m]	194	56	12	29
Net reservoir thickness [m]	82	47	7	24
Net pay thickness [m]	33	5	4	17
Gross porosity [%]	14	21	15	17
Average volume of shale [%]	53	59	40	50
Average water saturation [%]	55	62	50	55

Table 4

Reservoir properties in Lower Goru Sands in Siraj South-01 well

Siraj South-01	Upper sand	Middle sand	Sand above Talhar Shale	Basal sand
Depth range [m]	2383-2472	2597-2736	2905-2985	3055-3200
Gross thickness [m]	88	139	59	145
Net thickness [m]	79	35	18	66
Net reservoir thickness [m]	20	32	18	43
Net pay thickness [m]	7	5	18	30
Gross porosity [%]	8	23	17	13
Average volume of shale [%]	50	60	65	46
Average water saturation [%]	56	60	30	35

Table 5

Thickness of different shales in Upper and Basal sand level using data from Figs. 9 and 15a in Siraj South-01 well

Shale type	Upper sand thickness [m]		Basal sand thickness [m]
Laminated shale	6		35
Dispersed shale	Pore filling	28	23
	Grain replacing	19	18

persed shale at Upper sand level as compared to the structural and laminar shales (Table 5). This reduces porosity and increases water saturation at Upper sand level along with the effects of structural (may or may not affect res-

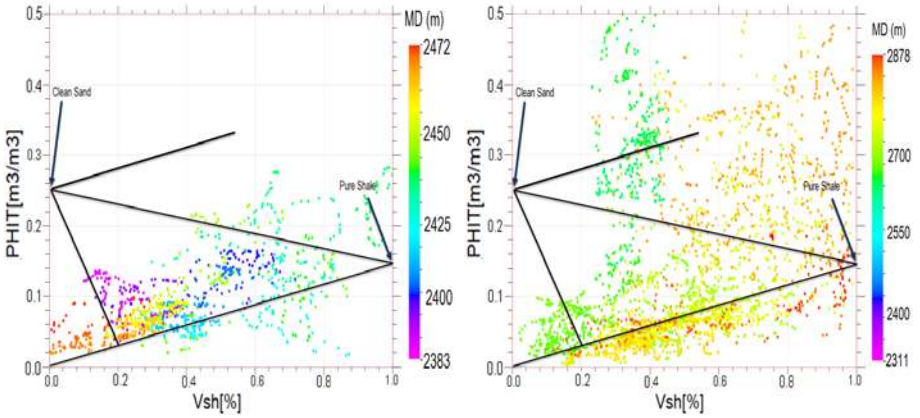

Fig. 9. Shale distribution at Upper sand level in well Siraj South-01 (left) and Naimat Basal-01 (right). Figure 5 is used as a reference for the interpretation of the above cross-plots.

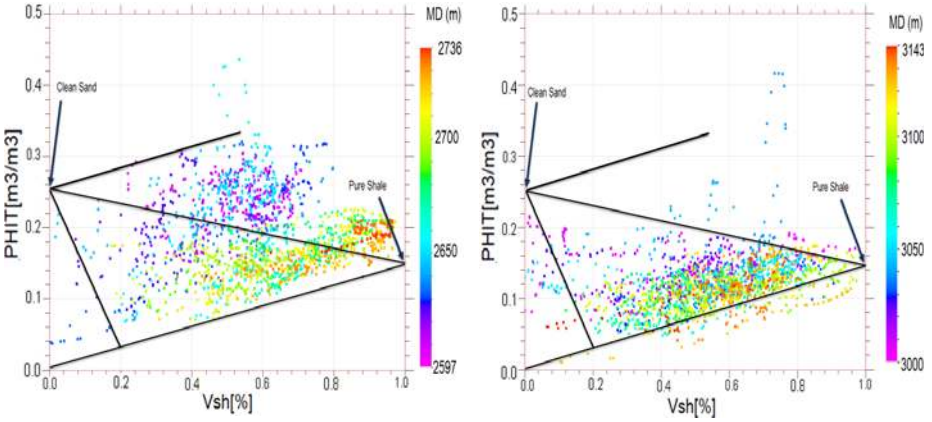

Fig. 10. Shale distribution at Middle sand level in well Siraj South-01 (left) and Naimat Basal-01 (right). Figure 5 is used as a reference for the interpretation of the above cross-plots.

ervoir properties) and laminated shale (only affects the vertical reservoir properties). On the other hand, Basal sand consists mainly of laminar shale along with significant amount of dispersed shale (Table 5). The presence of more laminar shale at Basal sand level as compared to Upper sand level is probably one of the reasons that Basal sand is a major producer in most of the drilled wells in the study area.

A detailed sand-shale analysis was carried out at Basal sand level, which helps in differentiating between hydrocarbon (oil/gas) and non-hydrocarbon

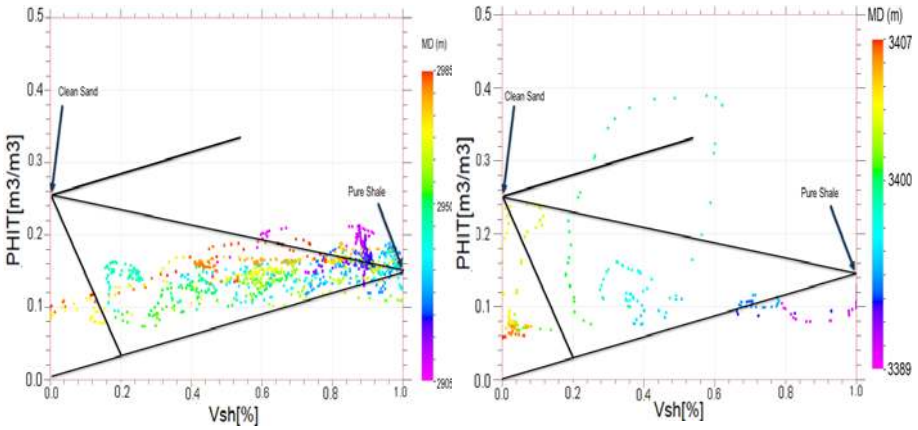

Fig. 11. Shale distribution at Sand above Talhar Shale in well Siraj South-01 (left) and Naimat Basal-01 (right). Figure 5 is used as a reference for the interpretation of the above cross-plots.

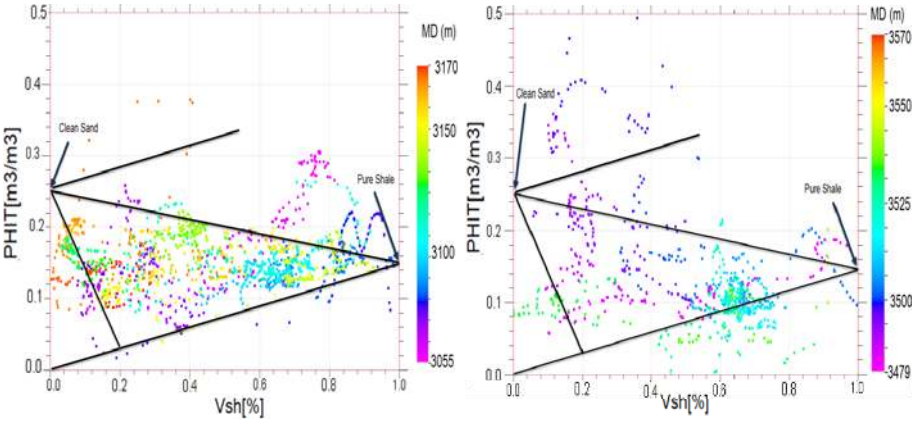

Fig. 12. Shale distribution at Basal sand level in well Siraj South-01 (left) and Naimat Basal-01 (right). Figure 5 is used as a reference for the interpretation of the above cross-plots.

(water) bearing sands using the data of Siraj-South-01 well. The cross-plots of laterolog deep resistivity (LLD), gamma ray (GR) log, and neutron porosity log (NPHI) were used for this purpose. In hydrocarbon bearing formation, the resistivity log signatures show high resistivity values than in water bearing formation (Fig. 13). On the cross-plot of the NPHI *versus* GR using the data of Siraj-South-01 well, we can identify the clean/gas sands at low neutron porosity and low gamma ray value (Fig. 14).

The results obtained from sand-shale analysis (Figs. 13-14) and types of shale distribution at Basal sand level (Fig. 15a) were integrated with the

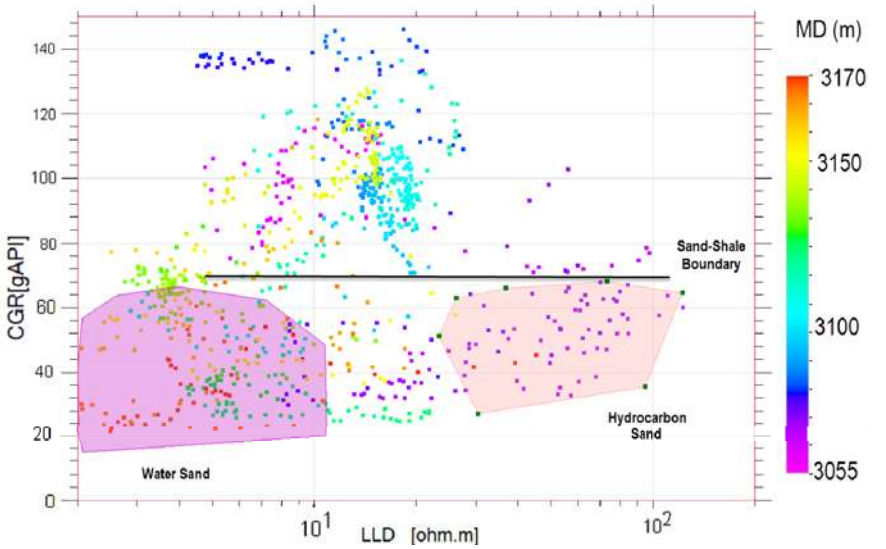

Fig. 13. Detailed sand-shale analysis using the cross-plot of LLD *versus* GR from Siraj South-01 well for the identification of hydrocarbon and water bearing sand at Basal sand level.

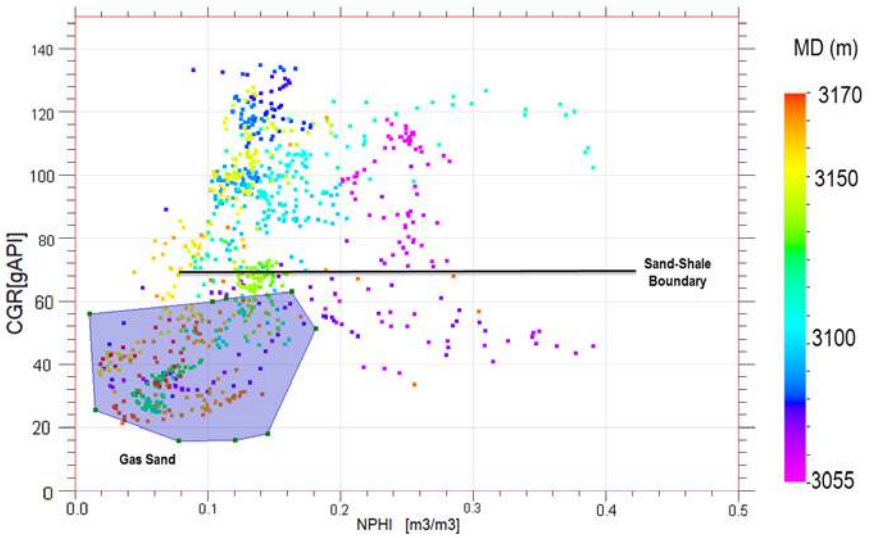

Fig. 14. Detailed sand-shale analysis using the cross-plot of NPHI *versus* GR from Siraj South-01 well for the identification of hydrocarbon and water bearing sand at Basal sand level.

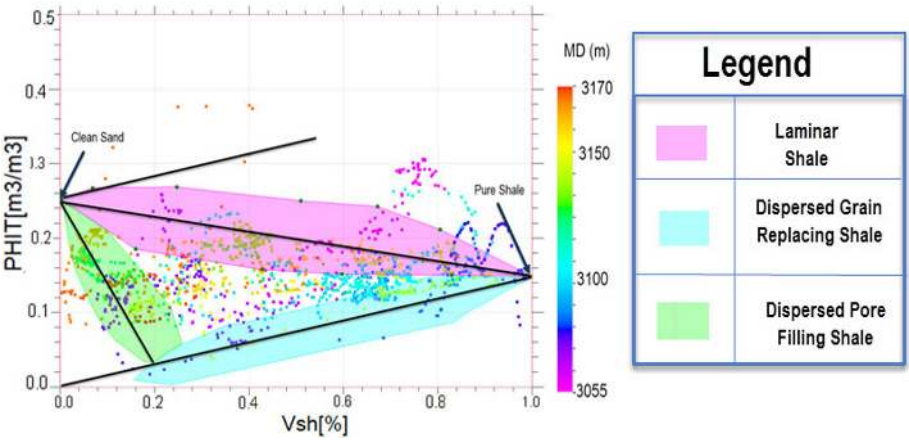

Fig. 15a. Shale distribution at Basal sand level in well Siraj-South-01. Polygons are drawn with reference to Fig. 5 with area between them showing mixture of different shale distributions.

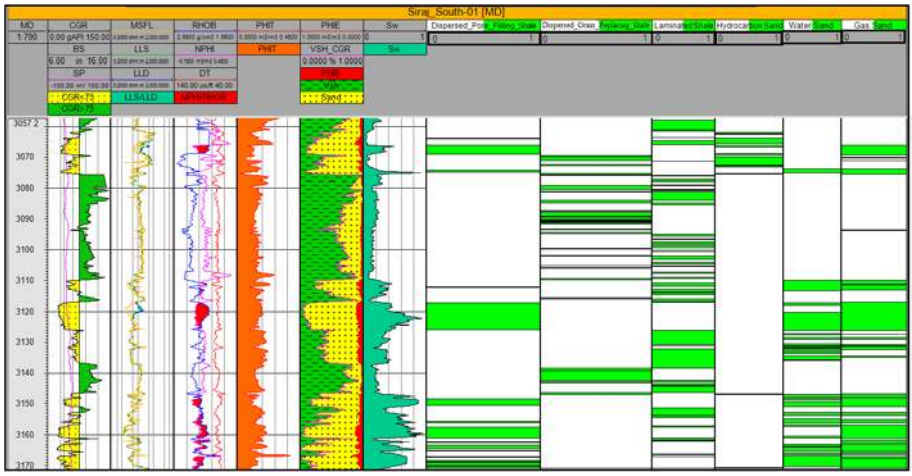

Fig. 15b. Petrophysical interpretation at Basal sand level in Siraj South-01 well showing consistent results (data within polygons of Figs. 13-15a) with Figs. 13-15a.

petrophysical interpretation. Clearly the density-porosity cross-over confirms the presence of hydrocarbons (Fig. 15b). There are different depth ranges that confirm presence of water sand and laminar shale (Fig. 15b) consistent with Figs. 13-15a.

5. ANISOTROPIC ROCK PHYSICS BASED AVA MODELLING FOR BASAL SAND

The purpose of this modeling at producing Basal sand level was to identify the class of sand based on AVA response (Rutherford and Williams 1989, Sen 2006). A further aim was to present an application of anisotropic rock physics modeling to generate AVA response based on the type of shale distribution. In reality, shales are often found to behave elastically as transversely isotropic media with a vertical axis of symmetry (Jakobsen and Johansen 1999, 2000). From rock physics modeling point of view, shales can be modeled as layers or in the form of lenses within the host medium (Sayers 1998). For modeling shales as thin layers within the host medium (sand), one can use the Backus averaging typically designed for layered medium modeling (Jakobsen *et al*. 2003, Ali *et al*. 2015, Sayers 1998, Backus 1962). Shales in the form of lenses within the host medium (sand) can be modeled with the help of inclusion based methods (Jakobsen *et al*. 2003, Ali *et al*. 2011). Here in our study area mainly laminar shale along with the dispersed shale are distributed in Basal sand layer. Laminar shale generally fulfills the criteria of being deposited in the form of thin layers. Therefore, the best available choice for rock physics modeling of shales in this study is using a laminar/layered model performed through the Backus averaging.

Shale layers within the sand matrix often show horizontally aligned orientation, thus making a transversely isotropic (TI) medium with a vertical axis of symmetry also known as VTI medium characterized either in terms of five independent elastic/stiffness constants (C_{11}, C_{13}, C_{33}, C_{55}, and C_{66}) or of two vertical velocities (V_P and V_S) and three Thomsen anisotropic parameters (γ, δ, ε) (Thomsen 1986, Tsvankin 1997a, b; Ali *et al*. 2011).

The effective stiffness of a stratified medium composed of transversely isotropic layers in the limit of long-wavelength is also effectively anisotropic and is given by Backus (1962)

$$\begin{bmatrix} A & B & F & 0 & 0 & 0 \\ B & A & F & 0 & 0 & 0 \\ F & F & C & 0 & 0 & 0 \\ 0 & 0 & 0 & D & 0 & 0 \\ 0 & 0 & 0 & 0 & D & 0 \\ 0 & 0 & 0 & 0 & 0 & M \end{bmatrix}, \qquad M = \frac{1}{2}(A - B), \tag{1}$$

where A, B, C, D, and F are the five independent effective elastic constants. In terms of P- and S-wave velocities (V_P and V_S) and densities (ρ), the five independent elastic constants can be written as

$$A = \left\langle 4\rho V_S^2 \left[1 - \frac{V_S^2}{V_P^2} \right] \right\rangle + \left\langle 1 - 2\frac{V_S^2}{V_P^2} \right\rangle^2 \left\langle \left(\rho V_P^2 \right)^{-1} \right\rangle^{-1}, \tag{2}$$

$$B = \left\langle 2\rho V_S^2 \left[1 - \frac{2V_S^2}{V_P^2} \right] \right\rangle + \left\langle 1 - 2\frac{V_S^2}{V_P^2} \right\rangle^2 \left\langle \left(\rho V_P^2 \right)^{-1} \right\rangle^{-1}, \tag{3}$$

$$C = \left\langle \left(\rho V_P^2 \right)^{-1} \right\rangle^{-1}, \tag{4}$$

$$F = \left\langle 1 - 2\frac{V_S^2}{V_P^2} \right\rangle^2 \left\langle \left(\rho V_P^2 \right)^{-1} \right\rangle^{-1}, \tag{5}$$

$$D = \left\langle \left(\rho V_S^2 \right)^{-1} \right\rangle^{-1}, \tag{6}$$

$$M = \left\langle \rho V_S^2 \right\rangle. \tag{7}$$

The brackets $\langle \cdot \rangle$ indicate averages of the enclosed properties weighted by their volumetric proportions. The input parameters V_P, V_S, and ρ for calculation of constants A-M in Eqs. 2-7 for the sand and shale layers at the Basal sand level are obtained from well log data of Siraj South-01 tabulated in Table 6. More specifically, we have used sonic and density log for the estimation of V_P and ρ at Basal sand level. As shear log was not available in any of the wells including Siraj South-01, we have estimated V_S from V_P for both sand and shale using relations given byMavko *et al*. (2009).

Once the five independent constants are obtained using the Eqs. 2-7 in our rock physics model, the Thomsen anisotropy parameters for VTI can be obtained using the relation given by Thomsen (1986, 1995)

Table 6

Mechanical properties used for anisotropic AVA modelling obtained from well Siraj South-01

Reservoir properties	Sand (matrix)	Shale (layers)	Overburden
P-wave velocity, V_P [m/s]	4355	3975	3970
S-wave velocity, V_S [m/s]	3403	2960	2250
Density, ρ [g/cm^3]	2.61	2.59	2.52
Porosity, φ (fraction)	0.09	0.11	–
Volume of shale, V_{sh} (fraction)	0.46	–	–
Water saturation, S_w (fraction)	0.18	–	–

$$\gamma = \frac{M - D}{2D} , \tag{8}$$

$$\varepsilon = \frac{A - C}{2C} , \tag{9}$$

$$\delta = \frac{(F + D)^2 - (C - D)^2}{2C(C - D)} . \tag{10}$$

In order to calculate the effect of fluid saturation on the effective properties of alternating sand shale layers, one can use the (anisotropic Gassmann) relations of Brown and Korringa (1975) (also see Ali *et al*. 2011, Shahraini *et al*. 2011). The values of porosity, water saturation, and volume of shale have been used in anisotropic Gassmann relation from well data of Siraj South-01 at Basal sand level given in Table 6.

For the purpose of seismic modelling, there exist many approximations, but we have used Rüger's approximation of reflection coefficients for VTI medium, because the influence of anisotropy can be readily analyzed on AVA signatures (Rüger 2002). The Rüger's approximation gives reflection coefficients as a function of polar incidence angle (*i*) written as (Rüger 2002)

$$R_P^{\mathrm{VTI}}(i) = \frac{1}{2}\frac{\Delta Z}{\overline{Z}} + \frac{1}{2}\left\{\frac{\Delta V_{P0}}{\overline{V}_{P0}} - \left(\frac{2\overline{V}_{S0}}{\overline{V}_{P0}}\right)^2 \frac{\Delta G}{\overline{G}} + \Delta\delta\right\}\sin^2 i + \frac{1}{2}\left\{\frac{\Delta V_{P0}}{\overline{V}_{P0}} + \Delta\right\}\sin^2 i \tan^2 i . \tag{11}$$

Here Z is the P-wave impedance, G is the shear modulus, V_{P0} is the effective P-wave velocity obtained using $V_{P0} = \sqrt{C/\rho}$, and V_{S0} is the effective shear wave velocity obtained using $V_{S0} = \sqrt{D/\rho}$. The constants C and D are obtained using Eqs. 4 and 6. The constants and δ are the anisotropy parameters for VTI media and obtained using relations in Eqs. 9 and 10. Here symbol Δ denotes contrast across an interface $(\Delta Z = Z_2 - Z_1)$ and a bar over a symbol denotes the average $\left(\overline{Z} = (Z_1 + Z_2)/2\right)$, where subscript 1 corresponds to the upper-half space (which corresponds to the mechanical properties V_P, V_S, and ρ of overburden tabulated in Table 6), and subscript 2 corresponds to lower-half space (which corresponds to the effective mechanical properties V_P, V_S, and ρ at Basal sand level obtained using Backus averaging).

The workflow followed to obtain the AVA response at Basal sand level is given in Fig. 16. The background parameters used in the computation of anisotropic rock physics and seismic modeling are tabulated in Table 6 and obtained from the analysis of data of Siraj South-01 well. It is important to clarify that the mechanical properties of sand and shale given in Table 6 are average values from well log data of Siraj South-01. These values are used

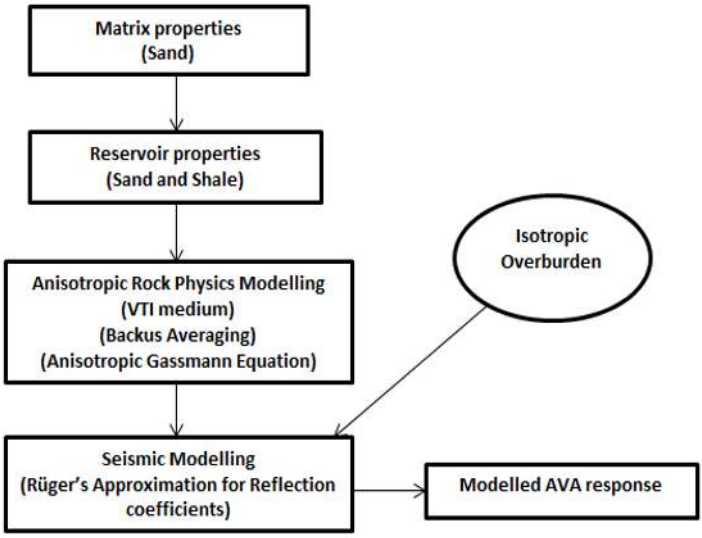

Fig. 16. Workflow followed for anisotropic rock physics based AVA modelling at Basal sand level.

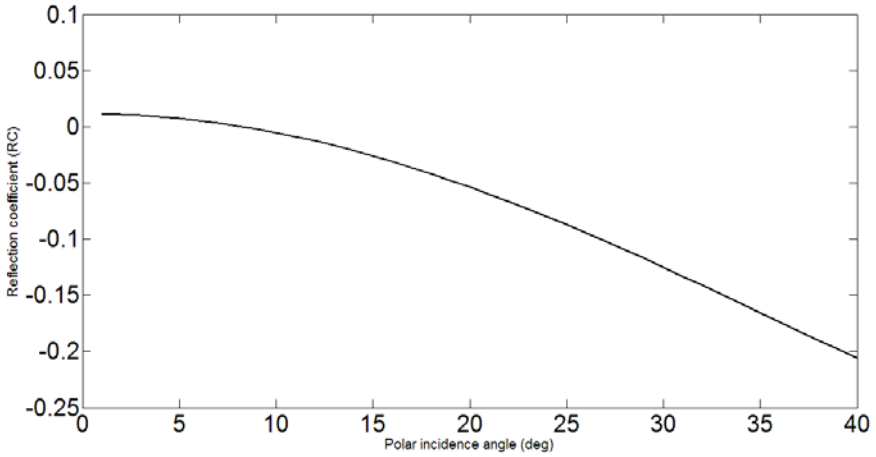

Fig. 17. Plot of reflection coefficient as a function of incidence angle at Basal sand level with $\delta = -0.008$ and $\varepsilon = 0.002$. Isotropic overburden is assumed during the computation with mechanical properties given in Table 6.

as an input by Backus averaging (Eqs. 1-10) to give effective mechanical properties at the Basal sand level. The overburden properties given in Table 6 represent the average mechanical properties obtained in lithologies above the Basal sand level using the well log data of Siraj South-01.

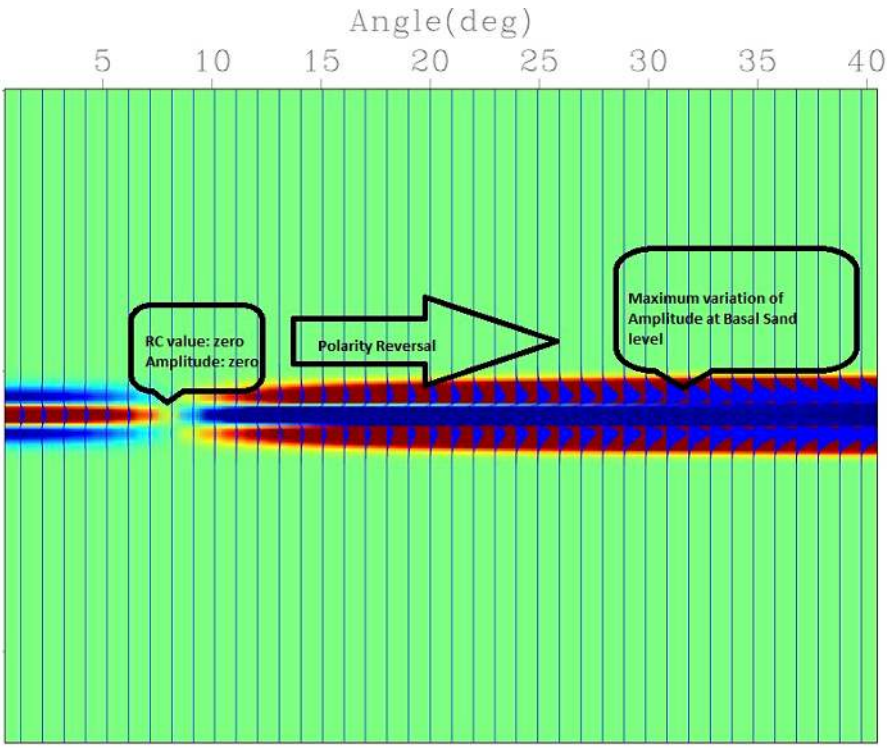

Fig. 18. Anisotropic AVA at Basal sand level. A polarity reversal at near offsets indicates moderately compacted AVO class II sand.

Figure 17 shows the reflection coefficients as a function of polar incidence for Basal sand level. There is a sharp decreasing trend of the reflection coefficients with the increasing angle of incidence (far offsets) at the Basal sand level. Figure 18 shows the AVA response at the top of the Basal sand level clearly indicating the polarity reversal due to negative reflection coefficients and maximum variation of amplitude at increasing polar angle of incidence (far offsets).

6. CONCLUSIONS

In this study we have presented a case study to determine the effect of shale distribution on producing sands from Khipro area, Lower Indus basin Pakistan using well log data. The well correlation using well tops at Lower Goru level reveals four sands (Upper sand, Middle sand, sand above Talhar shale, and Basal sand) and three shale (Upper shale, Lower shale, and Talhar shale) layers.

Based on the results of petrophysical analysis, Upper and Basal sand layers show very good reservoir quality in terms of net reservoir thickness and net pay thickness. We have also related the reservoir quality with the type of shale distribution within these two sand layers. Our results further reveal that there is a presence of more dispersed shale at Upper sand level as compared to the structural and laminar shales decreasing the porosity and increasing the water saturation. There is a presence of more laminar shale at Basal sand level as compared to dispersed shale, making this layer viable for hydrocarbon production.

A detailed sand-shale analysis based on LLD, GR, and neutron porosity logs integrated with petrophysical interpretation at the Basal sand level is also presented to discriminate between hydrocarbon and water bearing sands. The detailed sand-shale analysis and petrophysical interpretation results are consistent with each other at the Basal sand level.

We have also presented an anisotropic rock physics based AVA analysis at the Basal sand level using the workflow given in Fig. 16. Our analysis shows that due to negative reflection coefficients a polarity reversal can be observed at near incidence angles (near offsets) which indicate a moderately compacted AVO class II sand. The maximum variation of amplitude can be observed with increasing angle of incidence (far offsets). This way of modelling provides a framework for the calculation of anisotropic parameters (γ, δ, ε) required for anisotropic AVA. It will also improve the matching of amplitudes with the seismic gather at far offsets as compared to an isotropic AVA model where anisotropy is ignored.

Acknowledgments. Dr. Aamir Ali would like to thank the Directorate General of Petroleum Concessions (DGPC), Pakistan, for allowing the use of seismic and well log data for research and publication purposes and the Department of Earth Sciences, Quaid-i-Azam University, Islamabad, Pakistan for providing the basic requirements to complete this work.

References

Ahmad, N., P. Fink, S. Strurrock, T. Mahmood, and M. Ibrahim (2004), Sequence stratigraphy as predictive tool in Lower Goru Fairway, Lower and Middle Indus platform, Pakistan". **In:** *Proc. PAPG-SPE Annual Technical Conference, 8-9 October 2004, Islamabad, Pakistan*, 85-104.

Akhter, G., Z. Ahmed, A. Ishaq, and A. Ali (2015), Integrated interpretation with Gassmann fluid substitution for optimum field development of Sanghar area, Pakistan: A case study, *Arab. J. Geosci.* **8**, 9, 7467-7479, DOI: 10.1007/s12517-014-1664-8.

Ali, A., A. Shahraini, and M. Jakobsen (2011), Improved characterization of fault zones by quantitative integration of seismic and production data, *J. Geophys. Eng.* **8**, 2, 259, DOI: 10.1088/1742-2132/8/2/011.

Ali, A., M. Kashif, M. Hussain, J. Siddique, I. Aslam, and Z. Ahmed (2015), An integrated analysis of petrophysics, cross-plots and Gassmann fluid substitution for characterization of Fimkassar area, Pakistan: A case study, *Arab. J. Sci. Eng.* **40**, 1, 181-193, DOI: 10.1007/s13369-014-1500-1.

Asquith, G.B., D.A. Krygowski, S. Henderson, and N. Hurley (2004), *Basic Well Log Analysis*, American Association of Petroleum Geologists, 244 pp.

Backus, G.E. (1962), Long-wave elastic anisotropy produced by horizontal layering, *J. Geophys. Res.* **67**, 11, 4427-4440, DOI: 10.1029/JZ067i011p04427.

Bender, F.K., and H.A. Raza (1995), *Geology of Pakistan*, Borntraeger, Berlin.

Brown, R.J.S., and J. Korringa (1975), On the dependence of the elastic properties of a porous rock on the compressibility of the pore fluid, *Geophysics* **40**, 4, 608-616, DOI: 10.1190/1.1440551.

Clavaud, J.B., R. Nelson, U.K. Guru, and H. Wang (2005), Field example of enhanced hydrocarbon estimation in thinly laminated formation with a triaxial array induction tool: A laminated sand-shale analysis with anisotropic shale. **In:** *SPWLA 46th Annual Logging Symposium, 26-29 June 2005, New Orleans, USA*, SPWLA-2005-WW.

Clavier, C., G. Coates, and J. Dumanoir (1984), Theoretical and experimental bases for the dual-water model for interpretation of shaly sands, *Soc. Petrol. Eng. J.* **24**, 2, 153-168, DOI: 10.2118/6859-PA.

Heslop, K. (2005), *Interpretation of Shaly Sands*, London Petrophysical Society, London.

Jakobsen, M., and T.A. Johansen (1999), A test of ANNIE based on ultrasonic measurements on a shale, *J. Seism. Explor.* **8**, 1, 77-89.

Jakobsen, M., and T.A. Johansen (2000), Anisotropic approximations for mudrocks: A seismic laboratory study, *Geophysics* **65**, 6, 1711-1725, DOI: 10.1190/1.1444856.

Jakobsen, M., J.A. Hudson, and T.A. Johansen (2003), T-matrix approach to shale acoustics, *Geophys. J. Int.* **154**, 2, 533-558, DOI: 10.1046/j.1365-246X.2003.01977.x.

Kazmi, A.H., and I.A. Abbasi (2008), *Stratigraphy and Historical Geology of Pakistan*, Department and National Centre of Excellence in Geology, Peshawar, Pakistan.

Kurniawan, F. (2005), Shaly sand interpretation using CEC-dependent petrophysical parameters, Ph.D. Thesis, Louisiana State University and Agricultural and Mechanical College, Baton Rouge, USA.

La Vigne, J., M. Herron, and R. Hertzog (1994), Density-neutron interpretation in shaly sands. **In:** *Proc. SPWLA 35th Annual Logging Symp., 19-22 June, Tulsa, USA*, 16 pp.

Li, S., C.M. Henderson, and R.R. Stewart (2004), Well log study and stratigraphic correlation of the Cantuar Formation, southwestern Saskatchewan, *CREWES Res. Rep.* **16**, 1-18.

Mavko, G., T. Mukerji, and J. Dvorkin (2009), *The Rock Physics Handbook: Tools for Seismic Analysis of Porous Media*, 2nd ed., Cambridge University Press, Cambridge.

Minh, C.C., J.B. Clavaud, P. Sundararaman, S. Froment, E. Caroli, O. Billon, G. Davis, and R. Fairbairn (2008), Graphical analysis of laminated sand-shale formations in the presence of anisotropic shales, *Petrophysics* **49**, 5, 395-405.

Oldham, R.D. (1982), Report on the geology of Thal Chotiali and part of the Mari Country, *Records Geol. Survey India* **15**, 1, 18-29.

Paul, W.J. (2012), *Petrophysics,* Dept. of Geology and Petroleum Geology, University of Aberdeen.

Powell, C. (1979), A speculative tectonic history of Pakistan and surroundings: some constrains from Indian Ocean. **In:** A. Farah and K.A. De Jong (eds.), *Geodynamics of Pakistan*, Geological Survey of Pakistan, Quetta, 5-24.

Rüger, A. (2002), *Reflection Coefficients and Azimuthal AVO Analysis in Anisotropic Media*, Society of Exploration Geophysicists, Tulsa, 177-182, DOI: 10.1190/1.9781560801764.appd.

Rutherford, S.R., and R.H. Williams (1989), Amplitude-versus-offset variations in gas sands, *Geophysics* **54**, 6, 680-688, DOI: 10.1190/1.1442696.

Sams, M.S., and M. Andrea (2001), The effect of clay distribution on the elastic properties of sandstones, *Geophys. Prospect.* **49**, 1, 128-150, DOI: 10.1046/j.1365-2478.2001.00230.x.

Saxena, K., A. Tyagi, T. Klimentos, C. Morriss, and A. Mathew (2006), *Evaluating Deepwater Thin-Bedded Reservoirs with the RT Scanner*, Petromin, Kuala Lumpur.

Sayers, C.M. (1998), Long-wave seismic anisotropy of heterogeneous reservoirs, *Geophys. J. Int.* **132**, 3, 667-673, DOI: 10.1046/j.1365-246X.1998.00456.x.

Sen, M.K. (2006), *Seismic Inversion*, Society of Petroleum Engineers, Richardson, USA.

Shahraini, A., A. Ali, and M. Jakobsen (2011), Seismic history matching in fractured reservoirs using a consistent stiffness-permeability model: Focus on the effects of fracture aperture, *Geophys. Prospect.* **59**, 3, 492-505, DOI: 10.1111/j.1365-2478.2010.00934.x.

Sunjay, S. (2011), Shale gas: An unconventional reservoir, Department of Geophysics, Banaras Hindu University, Varanasi, India.

Tearpock, D.J., and R.E. Bischke (1991), *Applied Subsurface Geological Mapping,* Prentice-Hall, Inc., Englwood Cliffs.

Thomas, E.C., and S.J. Stieber (1975), The distribution of shale in sandstones and its effect on porosity. **In:** *Trans. SPWLA 16th Annual Logging Symp., 4-7 June 1975*.

Thomsen, L. (1986), Weak elastic anisotropy, *Geophysics* **51**, 10, 1954-1966, DOI: 10.1190/1.1442051.

Thomsen, L. (1995), Elastic anisotropy due to aligned cracks in porous rock, *Geophys. Prospect.* **43**, 6, 805-829, DOI: 10.1111/j.1365-2478.1995.tb00282.x.

Tiab, D., and E.C. Donaldson (2003), *Petrophysics: Theory and Practice of Measuring Reservoir Rock and Fluid Transport Properties*, Gulf Professional Publ., Waltham.

Tsvankin, I. (1997a), Anisotropic parameters and P-wave velocity for orthorhombic media, *Geophysics* **62**, 4, 1292-1309, DOI: 10.1190/1.1444231.

Tsvankin, I. (1997b), Reflection moveout and parameter estimation for horizontal transverse isotropy, *Geophysics* **62**, 2, 614-629, DOI: 10.1190/1.1444170.

Tyagi, A.K., R. Guha, D. Voleti, and K. Saxena (2009), Challenges in the reservoir characterization of a laminated sand shale sequence. **In:** *Proc. 2nd SPWLA-India Regional Symp., 19-20 November 2009, Mumbai, India*.

Visser, J. (1998), Extensile hydraulic fracturing of (saturated) porous materials. Ph.D. Thesis, Department of Civil Engineering and Geosciences, Delft University, Delft, The Netherlands.

Wandrey, C.J., B.E. Law, and H.A. Shah (2004), Sembar Goru/Ghazij composite total petroleum system, Indus and Sulaiman-Kirthar geologic provinces, Pakistan and India, U.S. Geological Survey Bulletin, Report #B 2208-C, 23 pp.

Waxman, M.H., and L.J.M. Smith (1968), Electrical conductivities in oil-bearing shaly sands, *SPE J.* **8**, 2, 107-122.

Zaigham, N.A., and K.A. Mallick (2000), Prospect of hydrocarbon associated with fossil-rift structures of the southern Indus basin, Pakistan, *AAPG Bull*. **84**, 11, 1833-1848.

Zinszner, B., and F.M. Pellerin (2007), *A Geoscientist's Guide to Petrophysics*, Editions Technip, Paris.

Received 31 October 2014
Received in revised form 4 August 2015
Accepted 18 August 2015